INDERSCIENCE PUBLISHERS
Linking academia, business and industry through research

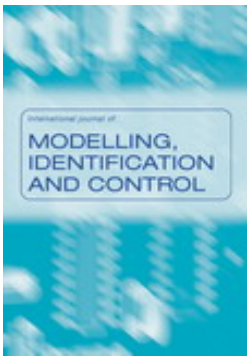

International Journal of Modelling, Identification and Control

ISSN online: 1746-6180 - ISSN print: 1746-6172
https://www.inderscience.com/ijmic

Online real-time prediction of propulsion speed for EPB shield machine by SSA-GRU

Wenshuai Zhang, Xuanyu Liu

DOI: 10.1504/IJMIC.2024.10064367

Article History:

Received:	06 October 2023
Last revised:	11 March 2024
Accepted:	27 March 2024
Published online:	30 September 2024

Online real-time prediction of propulsion speed for EPB shield machine by SSA-GRU

Wenshuai Zhang and Xuanyu Liu*

School of Information and Control Engineering,
Liaoning Petrochemical University,
Liaoning Fushun, 113001, China
Email: wenshuai991210@163.com
Email: yewil9924@163.com
*Corresponding author

Abstract: Given the extremely complex working environment of the shield machine, precise control of the digging parameters is the guarantee for the shield operation's safety. Therefore, the paper presents a sparrow search algorithm-gate recurrent unit (SSA-GRU) based online prediction approach for shield machine propulsion speed. Firstly, the construction data are correlated based on the Pearson correlation coefficient, to obtain the boring parameters that are highly correlated with the propulsion speed and are considered as input variables for prediction model. Secondly, SSA is utilised to find the optimal hyperparameters of model. Finally, a prediction model is established based on optimal hyperparameters found by SSA, which more precisely exploits the nonlinear relationship from input features with propulsion speed, and accurately predicts propulsion speed. Simulation findings demonstrate that SSA-GRU model can precisely predict propulsion speed, and the prediction performance is superior to that of other models, effectively maintaining the stability of the excavation surface.

Keywords: sparrow search algorithm-gate recurrent unit; SSA-GRU; propulsion speed; online real-time prediction.

Reference to this paper should be made as follows: Zhang, W. and Liu, X. (2024) 'Online real-time prediction of propulsion speed for EPB shield machine by SSA-GRU', *Int. J. Modelling, Identification and Control*, Vol. 45, No. 1, pp.19–30.

Biographical notes: Wenshuai Zhang obtained his Master's degree in Detection Technology and Automation Equipment in Liaoning Petrochemical University. His research direction is the autonomous control of earth pressure balance of shield machine.

Xuanyu Liu obtained his Doctorate in Control Theory and Control Engineering from Dalian University of Technology. His research direction is the modelling and intelligent control of earth pressure balance shield machine.

1 Introduction

Earth pressure balance (EPB) shield machine is extensively used in subway and other tunnels by virtue of its high efficiency, security, and other construction characteristics (Kongshu et al., 2011; Yu et al., 2021). The shield machine manually adjusts the digging parameters as the main manipulation pattern, but the working environment for the shield machine is extremely complicated, resulting in pressure imbalance on the excavation surface due to the manual inability to adjust the digging parameters in time, which causes safety accidents such as deformation of the ground surface to occur (Chen et al., 2019a). The EPB state is depicted in Figure 1. Therefore, it is meaningful to control the propulsion speed for the shield machine in a scientific and reasoned way (Li and Gong, 2020).

Figure 1 Shield machine earth pressure balance illustration (see online version for colours)

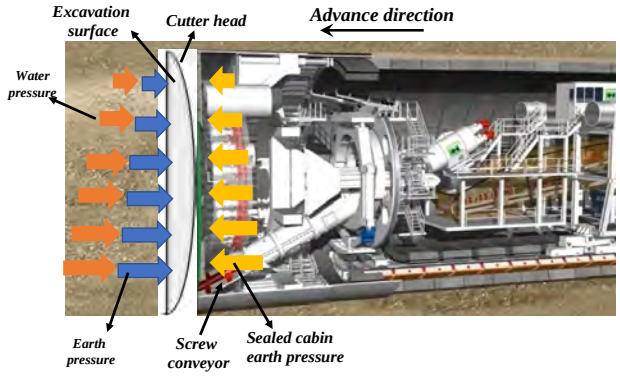

Precise controlled sealed cabin pressure and its dynamical equilibrium with excavation surface pressure are prerequisites for safe tunnelling. Adjusting the digging parameters by manual experience has many uncontrollable

factors, which can't timely adapt to the complicated and changeable environment in digging, and then it is very easy to cause safety accidents. It is evident that a scientific and precise prediction for shield tunnelling parameters has become a hot issue for scholars at home and abroad to carry out research (Guo et al., 2023; Huang et al., 2022; Hussaine and Mu, 2022). Yeh (1997) applied back propagation (BP) network to the prediction of sealed cabin pressure for an initial time, pioneering data-driven prediction in the shield machine area. Li and Gong (2019) established a prediction model for sealed cabin pressure on the basis of a diagonal recurrent neural network (DRNN). Liu et al. (2022b) established a multi-point sealed cabin pressure prediction model of discrete wavelet transform-deep convolutional neural network-long short-term memory (DWT-DCNN-LSTM), which realised the prediction of sealed cabin pressure. An intelligent prediction model of screw machine rotational speed based on convolutional neural network-gated recurrent unit (CCN-GRU) was proposed by Liu et al. (2022a) to predict screw conveyor speed. Zhang et al. (2023) proposed a thrust forecast method using SSA-LSTM for controlling sealed cabin pressure by adjusting the thrust magnitude. Song et al. (2019) constructed a thrust prediction model based on support vector regression (SVR) to accurately regulate the shield machine thrust. Armaghani et al. (2019) established a digging speed prediction model based on two hybrid optimisation methods. Chen et al. (2019a) proposed a blade torque and thrust prediction approach by LSTM. The above prediction model, based on basic data-driven approaches, typically utilises raw construction data to complete prediction tasks. However, due to the complex and variable geological environment ahead of the shield machine, the model trained on historical data struggles to capture the intricate influence of geological environment changes on propulsion speed, resulting in a lack of real-time prediction parameters. Additionally, the network structure parameters cannot be optimally adjusted, and the model fails to accurately capture data characteristics, leading to insufficient prediction accuracy. In addition, literature (Li and Gong, 2019; Yeh, 1997), the two models have a simple network structure and cannot effectively capture key features. In addition, the two models are prone to gradient disappearance or gradient explosion during training, resulting in the model unable to effectively learn the characteristics of the data, resulting in poor prediction accuracy. Furthermore, artificial intelligence methods are not only widely applied in other areas of shield tunnelling machines (Chen et al., 2023; Pan and Zhang, 2022; Qin et al., 2022), but also have significant achievements in materials and new instruments. Ma et al. (2023) proposed a prediction model for the remaining life of supercapacitors based on Harris hawks-long-short term memory (HHO-LSTM). Liu et al. (2023) used different principles to classify Electrochemical impedance spectroscopy (EIS) measurement methods and further explored the mechanism relationship between EIS and Lithium-ion batterie (LIB) aging effect. Yi et al. (2023) introduced a variety of measurement methods for the above parameters of various new energy storage devices, and summarised the advantages and disadvantages of the current research. Yu et al. (2023) expounded the feasibility of the application of nanogenerator technology in the field of acoustics and the flexibility of the combination of nanogenerator and acoustic equipment, and promoted the development of new energy storage devices and evaluation methods.

Aiming at the lack of real-time tunnelling parameters and the lack of model prediction accuracy, this paper proposes an online real-time prediction model of shield propulsion speed based on SSA-GRU, which realises online real-time prediction of propulsion speed according to tunnelling parameters collected by the host computer, and then accurately controls the sealed cabin pressure. Firstly, the construction data of the first two rings are temporalised to constitute a new time-series dataset. Secondly, SSA searches for the best hyperparameters of the GRU model obtained by global optimisation. This results in more stable training of the prediction model, faster convergence, and maximises the predictive performances in the model. Finally, the SSA-GRU propulsion speed prediction model is constructed based on the best hyperparameters found by SSA. The SSA-GRU model predicts the propulsion speed based on 6-dimensional input feature variables and conducts online rolling prediction based on the real-time tunnelling data. This greatly improves the predictive precision of the model and effectively avoids security incidents resulting from time-lag and inaccuracies in the digging parameter.

2 Basic theory

2.1 Gated recurrent unit

GRU is a variant of recurrent neural network (RNN) that solves the RNN gradient vanishing and gradient explosion problems and can capture long-term dependencies in sequences by introducing a gating mechanism. GRU has an update gate and a reset gate, which control the network's information transfer and update state to better capture the dependency of the time-step distances in the time-series data. Figure 2 shows the interior architecture of the GRU.

Figure 2 GRU network interior architecture (see online version for colours)

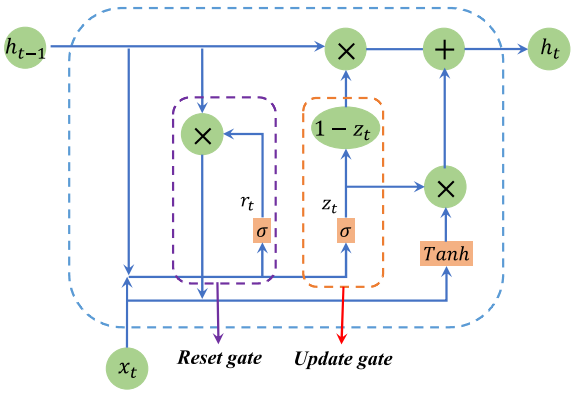

The reset gate is mainly used to determine the proportional weight of the hidden state from the previous time step as an input. A Sigmoid function is utilised to transform the hidden state h_{t-1} of the previous time step into the range [0, 1], which represents the proportion of the previous time state retained. The formula for the reset gate is:

$$r_t = \sigma\left(W_r \cdot [h_{t-1}, x_t] + b_r\right) \tag{1}$$

Based on equation (1), the candidate state $\tilde{h}_t$ of the hidden layer at the current time step can be calculated using the Tanh function with the formula:

$$\tilde{h}_t = tanh\left(W_h \cdot [h_{t-1}, x_t] + b_h\right) \tag{2}$$

The update gate is used to integrate the new input x_t in the current time step and the state h_{t-1} of the previous time. The data is converted to the range of [0, 1] by the Sigmoid function, which is used to determine the forgetting ratio of the information at the previous time and the retention ratio at the current time. The calculation formula is:

$$z_t = \sigma\left(W_z \cdot [h_{t-1}, x_t] + b_z\right) \tag{3}$$

$$h_t = (1 - z_t) * h_{t-1} + z_t * \tilde{h}_t \tag{4}$$

Among them, W_r, b_r are the weighing and bias matrices of the reset gate, x_t represents input vector, W_h, b_h are the weight matrix and bias matrix of the hidden layer, $\tilde{h}_t$ is the candidate state of the hidden layer, W_z, b_z are the weight matrix and bias matrix of the update gate, r_t, z_t are the input of the reset gate and the update gate respectively, h_t is the output value, * is the multiple operations of the correspondent components in the matrices.

Figure 3 SSA-GRU propulsion speed prediction scheme (see online version for colours)

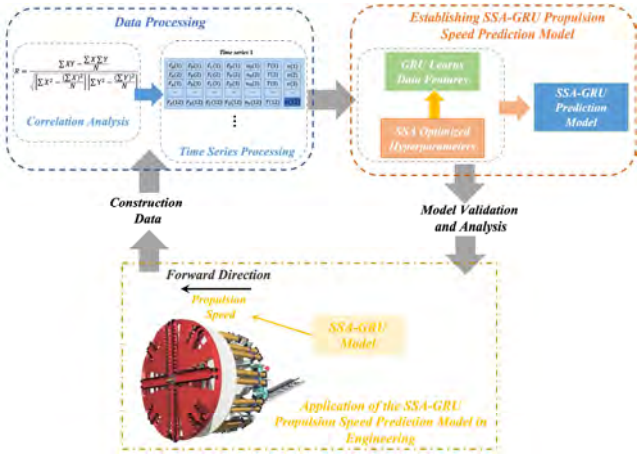

3 Prediction scheme

The prediction model is built based on SSA and GRU for shield machine propulsion speed to realise the online prediction and control of the propulsion speed. This prediction approach could precisely predict the propulsion speed on the basis of the historical parameter information. The predictive program is illustrated in Figure 3, and consists of three sections:

1 Perform data process for constructional data, determine input characteristic variables based on Pearson correlation analysis, and construct the time series.

2 Establish the GRU propulsion speed prediction model, and optimise the hyperparameters of the GRU model using SSA.

3 Examine the prediction performance of SSA-GRU from multiple angles based on actual construction data.

4 Data selection and processing

4.1 Selection of input data

In order to ensure excellent correspondence from input variables to propulsion speed and to make the prediction results more accurate, this paper analyses the construction databased on Pearson's correlation coefficient to determine the degree of correlation between each parameter of the shield machine and the propulsion speed, which enables an effective assessment and quantification of the degree of correlation between these parameters and the propulsion speed, and thus improves the accuracy of the prediction results.

$$R = \frac{\sum XY - \frac{\sum X \sum Y}{N}}{\sqrt{\left[\sum X^2 - \frac{\left(\sum X\right)^2}{N}\right]\left[\sum Y^2 - \frac{\sum (Y)^2}{N}\right]}} \tag{5}$$

where $R \in (-1, 1)$ is the Pearson correlation coefficient. N represents sample; Y represents propulsion speed; and X represents the value of the relevant variable in 10 dimensions. Pearson relation result among each parameter and propulsion speed is illustrated in Figure 4.

Figure 4 Thermogram of correlation coefficient (see online version for colours)

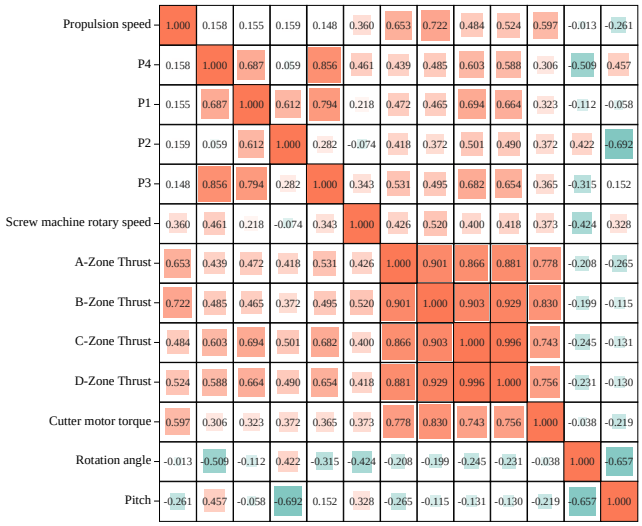

The results of Pearson's correlation analysis can be concluded that the correlation coefficients of F_A (A-zone thrust), F_B (B-zone thrust), F_C (C-zone thrust), F_D (D-zone thrust), screw conveyor rotary speed n_0, and cutter motor total torque T with propulsion speed are all above 0.35, which means that they show medium-strong correlation, and therefore, the above six-dimensional variables are served input features for predictive model. Shield machine thrust partition is shown in Figure 5.

Figure 5 Shield machine thrust partitioning schematic diagram (see online version for colours)

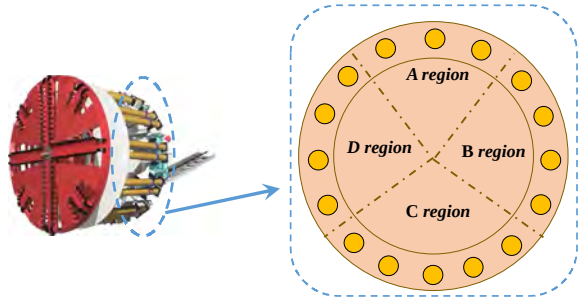

Figure 6 Data timing results (see online version for colours)

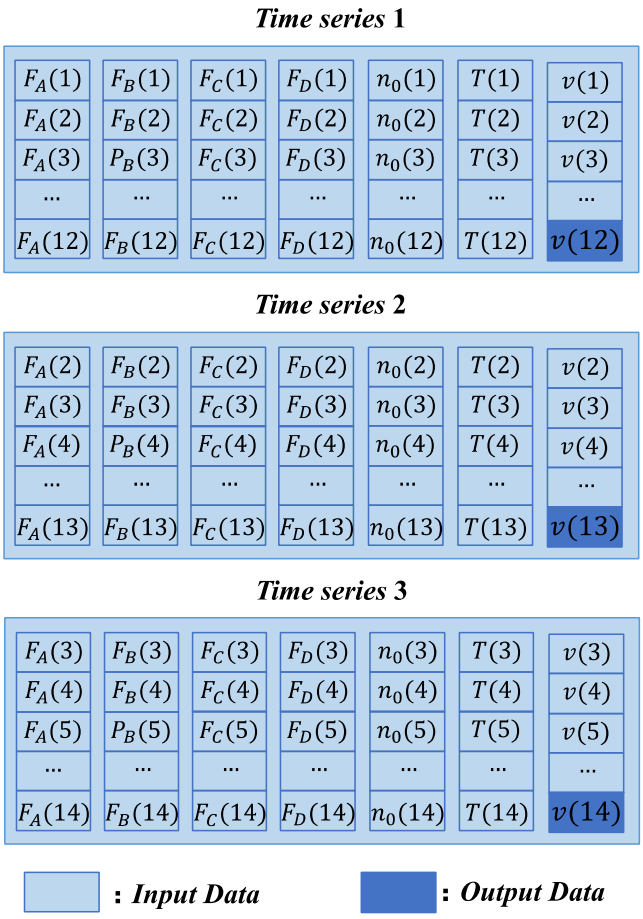

4.2 Constructing time series

Time series are compatible with the characteristics of the GRU model, which can utilise the recursive structure to efficiently process sequential data, thus better capturing the time dependency in the data. On the basis of this, this section temporalises the shield machine construction data into the input data form required by the GRU prediction model. The time-series building results are illustrated in Figure 6.

Each sequence consists of data over a range of time periods and input feature variables for the next moment, which are used to predict the propulsion speed. As an example, for time series 1–3, the first time series consists of data at times 1–11 and input feature variables at time 12 for predicting the shield machine propulsion speed at time 12. The second time series consists of data at times 2–12 and input feature variables at time 13 for predicting the shield machine propulsion speed at time 13. The third time series is composed of data for times 3–13 and input feature variables for time 14 to predict the shield machine propulsion speed for time 14. In this rolling way, multiple time series are gradually established, in which the input data of each sequence covers the data value of the previous moment and the input characteristic variables of the current moment, so as to predict the propulsion speed at the current moment and provide an accurate basis for subsequent analysis and prediction. The corresponding predictive model formulation is depicted as equation (6).

$$\begin{aligned} v(k) = f\big(&F_A(k-11), F_A(k-10), F_A(k-9), \cdots, F_A(k),\\ &F_B(k-11), F_B(k-10), F_B(k-9), \cdots, F_B(k),\\ &F_C(k-11), F_C(k-10), F_C(k-9), \cdots, F_C(k),\\ &F_D(k-11), F_D(k-10), F_D(k-9), \cdots, F_D(k),\\ &n_0(k-11), n_0(k-10), n_0(k-9), \cdots, n_0(k),\\ &T(k-11), T(k-10), T(k-9), \cdots, T(k),\\ &v(k-11), v(k-10), v(k-9), \cdots, v(k-1)\big) \end{aligned} \tag{6}$$

where k is the predicted moment; $FA(k)$, $F_B(k)$, $F_C(k)$, $F_D(k)$ are the four regions thrust values of the shield machine for the training sequence; $v(k–11)$, $v(k–10)$, $v(k–9)$, …, $v(k–1)$ are the propulsion speed for training sequence; $n_0(\cdot)$, $T(\cdot)$ represent the screw conveyor speed and the total torque of the cutter disk, respectively.

5 Model establishment and training

5.1 Establishing SSA-GRU predictive modelling

The propulsion speed prediction model is composed of four parts: input layer, hidden layers 1 and 2, and output layer. Figure 7 shows network structure. Input layer is the 6-dimensional input characteristic variable selected in Section 4.1, and output layer is propulsion speed.

Figure 7 SSA-LSTM prediction model network structure diagram (see online version for colours)

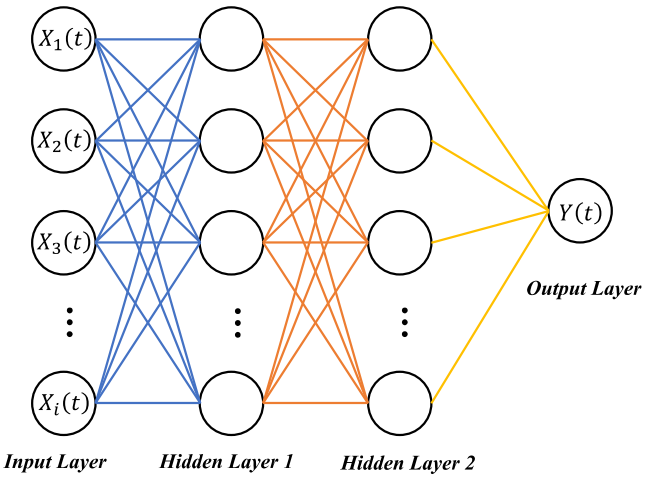

where $X_i(t)$ is a 6-dimensional input feature variable, i = 6. $Y(t)$ is the predicted value of the propulsion speed. t is a time series value. The number of neurons in hidden layer 1 and hidden layer 2, the learning rate of the prediction model, and the number of iterations are obtained by the global optimisation search of the SSA algorithm.

5.2 *Determination of hyperparameters for GRU model*

SSA is an intelligent bionic optimisation algorithm based on the foraging and anti-predator behaviour of the sparrow and categorises it into producers and dabblers based on their biological characteristics. The producers usually have a high level of energy reserves and provide foraging direction to all foragers, whose position changes as:

$$X_{i,j}^{t+1} = \begin{cases} X_{i,j}^{t} \cdot exp\left(\dfrac{-i}{\alpha \cdot M}\right) & if\ R^* < ST \\ X_{i,j}^{t} + Q \cdot L & if\ R^* \geq ST \end{cases} \tag{7}$$

where t is iterations. i is the number for individuals. j represents the population dimension. $X_{i,j}^{t}$ represents the position in the j^{th} dimension at iteration t for the i^{th} sparrow individual. α is random number. M is maximum iteration number. R^* represents alarm value. ST represents the safety threshold. Q represents the random number. L denotes the 1-dimensional matrix.

In natural state, dabblers follow the producer who provides the best food in search of food, and in the process, dabblers constantly monitor the producer and compete for food to increase their predation rate. Its position changes as follows:

$$X_{i,j}^{t+1} = \begin{cases} Q \cdot exp\left(\dfrac{X_w - X_{i,j}^{t}}{i^2}\right) & if\ i > \dfrac{n}{2} \\ X_P^{t+1} + \left|X_{i,j}^{t} - X_P^{t+1}\right| \cdot A^+ \cdot L & Other \end{cases} \tag{8}$$

where X_P represents the best position occupied by the producer. X_w represents the current global worst position. A represents a one-dimensional matrix. $A^+ = A^T(AA^T)^{-1}$.

When the vigilantes realise the danger, they will immediately sound the alarm, and sparrows located around the margins of the flock would move to safety rapidly for a better place, whereas those located at the centre would randomised to move closer to the other sparrows. The position changes are:

$$X_{i,j}^{t+1} = \begin{cases} X_B^{t} + \beta \cdot \left|X_{i,j}^{t} - X_B^{t}\right| & if\ f_i > f_g \\ X_{i,j}^{t} + K \cdot \left(\dfrac{\left|X_w - X_{i,j}^{t}\right|}{(f_i - f_w) + \varepsilon}\right) & if\ f_i = f_g \end{cases} \tag{9}$$

where β is the step control parameter. $K \in (-1, 1)$. f_g represents the best-adapted value of authority. f_w represents the worst adapted value of the authority. ε is the smallest constant that avoids division by zero. X_B^{t} represents the safest centre position.

Based on the SSA algorithm, the four hyperparameters of the GRU prediction model, namely, the number of iterations, the learning rate, the number of neurons in the hidden layer 1 and the hidden layer 2, are used for global optimisation, in which the search ranges of the four hyperparameters are, respectively, [1, 100], [0.001,0.01], [1, 100], [1, 100]. The parameters used in the SSA algorithm are depicted in Table 1. The process for SSA searching for optimal GRU model hyperparameters is:

- Input: M: iteration number of SSA algorithm. *pop*: sparrow population sise. *P_*: sparrow population proportion accounted for by producers. *dim*: merit seeking dimension, search interval.
  1. SSA identifies the GRU network topology.
  2. Real-time construction data input to SSA algorithm.
  3. Initialise the weights and biases of the GRU.
  4. Calculate fitness values for the area in which the stock is found.
  5. Continuously update location information of producers, dabblers, and alarms based on equations (7)–(9).
  6. Determine whether the fitness value satisfies the termination condition; if it does, output the best hyperparameters; otherwise, continue iterating.
- Output: The best hyperparameters of the model: The optimal hyperparameters found by SSA for the prediction model are listed in Table 2.

Table 1 SSA algorithm parameters

Iteration number	20
Sparrow population	10
Search for optimisation dimensions	4
Producers as a proportion of population	0.2

Table 2 Optimal hyperparameters for the prediction model

Iteration number	96
Learning rate	0.0089
Neuron number in hidden layer 1	70
Neuron number in hidden layer 2	55

The GRU model applies the best hyperparameters found by SSA and observes the trend in loss function curve of the model during its training process as a way to calibrate the reasonableness of the best hyperparameters found by SSA. Figure 8 illustrates the loss function variation curve for the predictive model.

Figure 8 Loss function variation curve (see online version for colours)

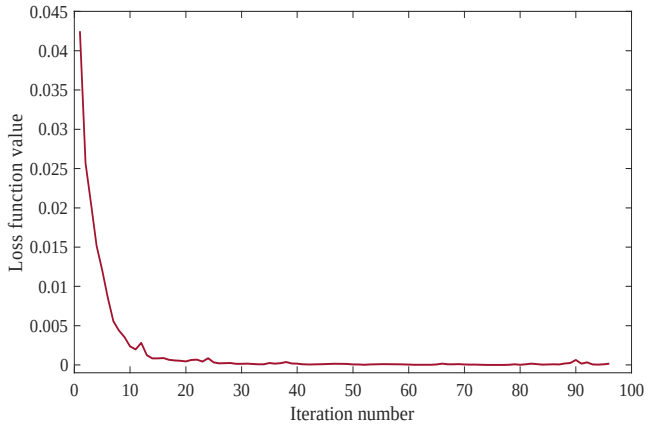

It can be observed from Figure 8 that within 1–10 iterations of the loss function curve, the fluctuation of the loss function is large and gradually decreases, but after 10 iterations, the loss function is gradually smoothed and tends to stabilise, and finally, the loss function converges to 0. It can be illustrated that the optimal hyperparameters found based on SSA for the GRU model can reach convergence quickly and the training process is stable.

5.3 SSA-GRU model prediction process

The prediction process is illustrated in Figure 9. By temporising the real-time construction data transmitted from the host computer and splitting it into the training set and test set, the SSA algorithm obtains the optimal hyperparameters of the GRU model through a global optimisation search. In the training process, iterates based on the training set and the optimal hyperparameters by continuously updating the weights and biases, thus completing the model training process. The trained prediction model is tested based on the test set, and the prediction performance is examined by analysing and comparing the relationship of predicted outcomes to actual values, so as to realise the online real-time prediction of the shield machine propulsion speed. The process is described below:

- Input: optimal hyperparameters for GRU model.
  1. Time-series the construction data transmitted from the host computer.
  2. Split the temporalised construction data into the training and test sets.
  3. Based on training set, train the GRU by continuously updating the weights and biases.
  4. GRU model training is completed.
  5. Test the trained GRU model based on the test set.
- Output: Shield machine propulsion speed.

Figure 9 SSA-GRU model prediction process (see online version for colours)

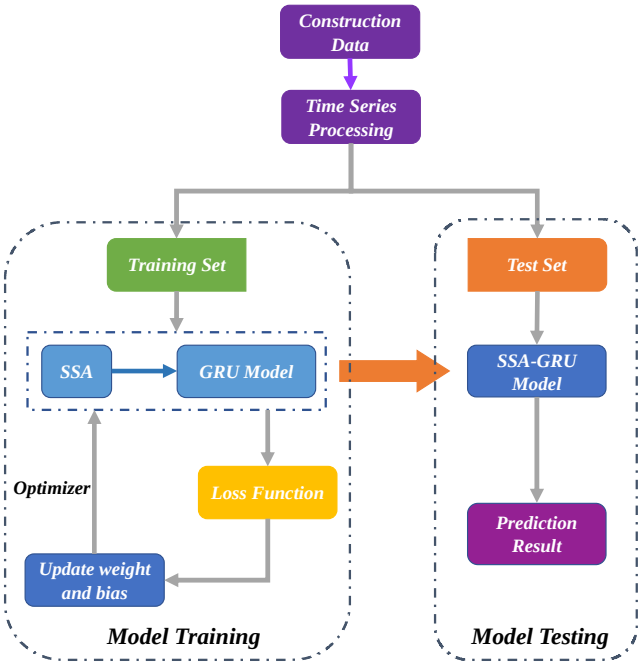

6 Analysis of simulation result

Experiments are carried out on a segment of Beijing Metro Line 10. This segment is a typically soft sandy rock layer. Tunnel geological section is shown in Figure 10. In this paper, PyCharm is used as the tool, and Python 3.8 and Tensorflow2.7.1 are used as the programming environment.

In the simulation, predictive model is trained using construction data from 202 and 203 rings, and the 204-ring data is used as the test. The model is tested in terms of prediction performance, predictive precision for the SSA-GRU model, and the effectiveness of the predicted data in controlling the sealed cabin pressure values.

Figure 10 Geological profile of tunnel (see online version for colours)

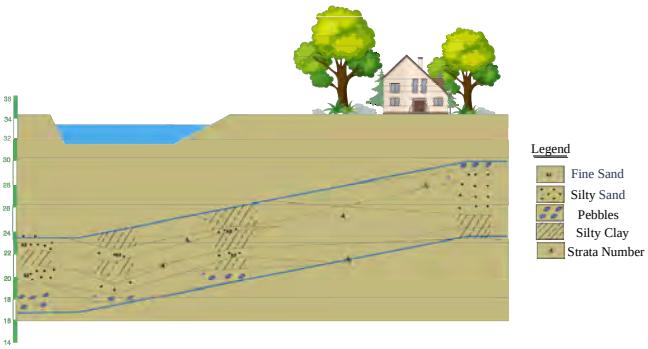

6.1 *The prediction accuracy test of SSA-GRU model*

Based on the prediction model established and trained in Section 5.1, the change in the shield machine's propulsion speed is predicted. The predictive accuracies of the prediction models were tested by comparing the prediction curves from the prediction models with the realistic curves. Figure 11 depicts the predicted outcome. The prediction error of propulsion speed is shown in Figure 12.

Figure 11 Prediction results of shield machine propulsion speed (see online version for colours)

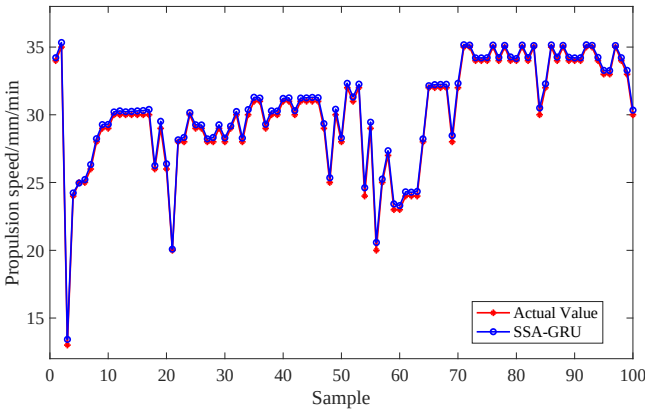

Figure 12 Prediction error of shield machine propulsion speed (see online version for colours)

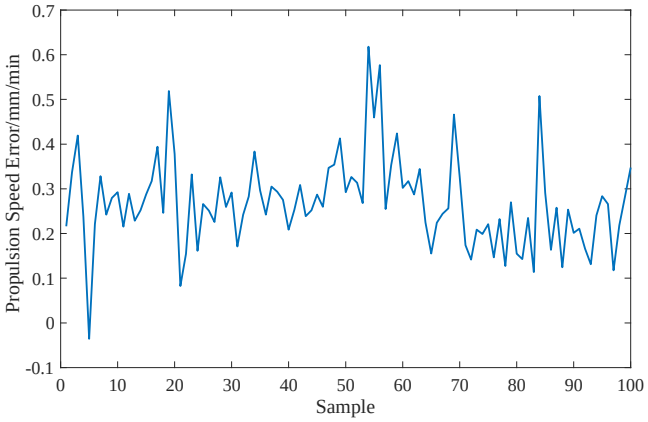

Figure 11 illustrates the real propulsion speed value curve and predictive value profile for SSA-GRU model. It can be evident from Figure 12 that the actual propulsion speed value curve has a good fitting degree with a predictive value profile, and the two are approximately coincident. It is clear from the prediction errors plot for shield propulsion speed that the deviation from the predicted and actual values is stabilised within the range of 0–0.6 mm/min, and the maximum error value of 0.6mm/min is within the allowable error range of the actual working condition. Consequently, the predictive model could fulfil the prediction task well.

Based on the above analysis, the error between the predicted value of the SSA-GRU model and the actual value is small, and the error is within the allowable range of the actual working conditions. It has high prediction accuracy and could fulfil the prediction mission well, so as to offer accurate and scientific reference for shield machine drivers.

6.2 *The superiority test of SSA-GRU model predictive effectiveness*

For testing the predictive effect of SSA-GRU, it is compared with the prediction effect of the MLP model, GRU model, and LSTM model based on the same dataset. As illustrated in Figure 13, the predictive effectiveness of SSA-GRU is compared with that of other models. The prediction error pairs are depicted in Figure 14.

Figure 13 Comparison chart of prediction effect (see online version for colours)

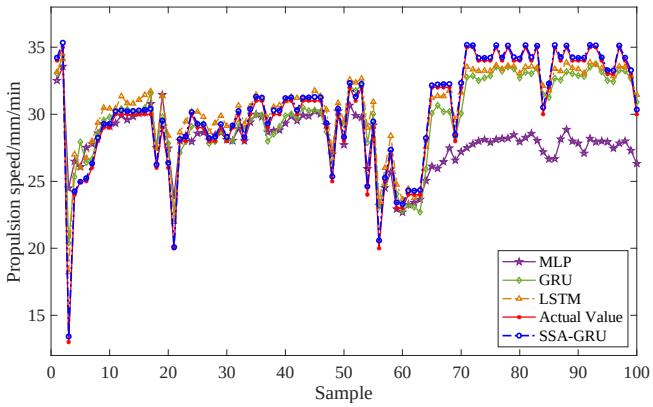

Figure 14 Comparison chart of prediction error (see online version for colours)

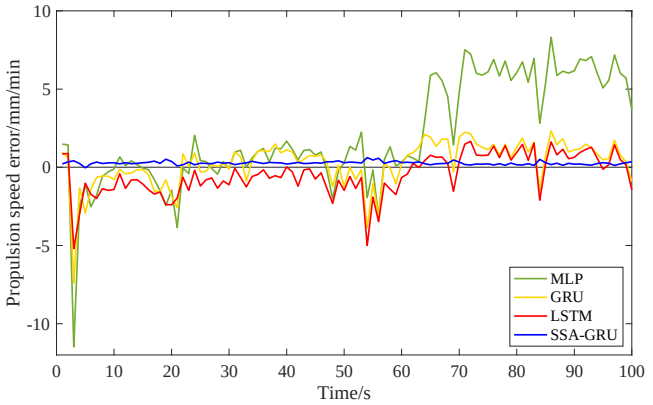

Table 3 The specific error data table of each model

Model error / *Sample*	*SSA-GRU*	*MLP*	*GRU*	*LSTM*
0	0.216045	1.480675236	0.953663	0.855934
1	0.336922	1.435157129	0.602837	0.88549
2	0.419333	–11.48477739	–7.395472	–5.210402
3	0.238134	–2.485767691	–1.322615	–3.007607
4	–0.035597	–1.074735561	–2.93284	–1.020491
5	0.221024	–2.522471087	–1.386417	–1.734568
6	0.328327	–1.778006103	–0.645502	–1.990347
7	0.242517	–0.577642881	–0.554783	–1.365452
8	0.2796	–0.290796512	–0.56716	–1.480667
9	0.292292	–0.105509814	–0.785543	–1.423479
10	0.215498	0.670341514	–0.127047	–0.419502
11	0.288824	0.093568484	–0.412762	–1.341349
12	0.228882	0.414070946	–0.363998	–0.820961
13	0.252077	0.165535967	–0.155552	–0.79727
14	0.287579	–0.055242798	–0.147415	–1.070702
15	0.317526	–0.151018773	–0.484133	–1.436188
16	0.394104	–0.782305414	–1.52619	–1.712334
17	0.246199	–1.487585203	–1.536921	–1.583443
18	0.518871	–2.453326161	–0.804459	–2.385826
19	0.378012	–1.462304572	–1.830719	–2.403313
20	0.082451	–3.855466893	–2.588327	–1.965855
21	0.154573	–0.03506709	0.868782	–0.643406
22	0.332239	–0.40380823	0.040115	–1.473625
23	0.161232	2.03782225	0.917246	–0.188763
24	0.265751	0.423717279	–0.290834	–1.188358
25	0.251358	0.363502358	–0.25795	–0.801533
26	0.225866	–0.072433864	0.184595	–0.679876
27	0.325502	–0.447820853	0.038019	–1.332609
28	0.259413	0.364001078	0.25433	–0.878769
29	0.291817	–0.096428539	–0.112684	–1.125235
30	0.171047	0.978810212	0.986423	–0.061544
31	0.242144	1.081705613	0.670765	–0.650314
32	0.282633	–0.005990059	–0.888323	–1.261
33	0.383543	0.592022926	0.410868	–0.59164
34	0.296421	1.002882801	1.044579	–0.454037
35	0.242361	1.206804589	1.066114	–0.162722
36	0.305056	0.336077878	1.009396	–0.703554
37	0.293406	1.220987256	1.485083	–0.537399
38	0.27527	1.184345497	0.92421	–0.666058
39	0.20854	1.673229721	1.11754	0.026472
40	0.252878	1.147268009	0.97575	–0.296717
41	0.308531	0.475262097	0.306021	–1.211391
42	0.238909	1.07483919	0.500557	–0.172665
43	0.252165	1.125893241	0.750298	–0.10161
44	0.287226	0.784517686	0.704235	–0.758327

Table 3 The specific error data table of each model (continued)

Model error / *Sample*	*SSA-GRU*	*MLP*	*GRU*	*LSTM*
45	0.259935	0.975199858	0.796543	–0.353956
46	0.347021	–0.203765684	0.309174	–1.337194
47	0.354221	–2.011061314	–1.237219	–2.312471
48	0.412849	–0.227300729	0.127678	–0.827929
49	0.292238	0.282565679	–1.224737	–1.4748
50	0.326359	1.338951057	–0.006866	–0.585651
51	0.313683	1.099662721	–0.770302	–1.358955
52	0.268051	2.245702717	–0.160046	–0.663204
53	0.618073	–1.935512868	–3.88377	–4.995924
54	0.459711	–0.175859786	–1.038925	–1.913052
55	0.57666	–3.183932557	–3.112686	–3.48107
56	0.254948	0.485617181	0.258036	–1.002911
57	0.353458	1.318779608	–0.060633	–1.387751
58	0.423853	0.079579457	–1.061836	–1.745846
59	0.302059	0.314935089	0.211861	–0.650282
60	0.31716	0.73706901	0.779045	–0.435814
61	0.287474	0.586578324	0.932001	0.246237
62	0.344294	0.361799473	1.295473	–0.02323
63	0.224949	2.949768806	2.103798	0.420481
64	0.155472	5.885148129	1.928877	0.764717
65	0.224007	6.042309575	1.335728	0.641376
66	0.243996	5.546544918	1.809624	0.65753
67	0.256191	4.524390013	1.807478	0.243723
68	0.466251	1.435285815	–0.269321	–1.534023
69	0.326218	4.804987243	1.934311	0.383579
70	0.173737	7.512054601	2.24086	1.473743
71	0.141598	7.232467646	2.132191	1.661625
72	0.208645	6.010298054	1.490185	0.78455
73	0.199093	5.890180215	1.287075	0.750923
74	0.220695	6.102881467	1.132732	0.77475
75	0.146454	6.886984638	1.466965	1.354843
76	0.232365	5.836946671	0.781944	0.618443
77	0.127197	6.795007066	1.477226	1.386894
78	0.269871	5.548194988	0.608028	0.449802
79	0.15501	6.054871319	1.291756	0.943989
80	0.142971	6.738349485	1.859783	1.466671
81	0.234818	5.442827258	0.969124	0.444202
82	0.113804	6.963150958	1.583977	1.535061
83	0.507664	2.817022453	–1.468025	–2.097504
84	0.290867	5.350914462	0.741636	0.212364
85	0.163609	8.315678614	2.322784	1.62249
86	0.257847	5.867158047	1.451355	0.793152
87	0.124352	6.144436277	1.822643	1.147213
88	0.253338	6.017471015	0.975777	0.549824
89	0.201561	6.17073301	1.115845	0.635033

Table 3 The specific error data table of each model (continued)

Model error / Sample	SSA-GRU	MLP	GRU	LSTM
90	0.210785	6.915080744	1.175266	0.941723
91	0.166237	6.815199784	1.479668	1.140095
92	0.131393	7.071992408	1.242393	1.28521
93	0.240601	6.0079836	0.838753	0.575165
94	0.283295	5.064402643	0.477539	–0.13208
95	0.265877	5.545238285	0.567226	0.169106
96	0.117832	7.176150898	1.726261	1.436081
97	0.218517	6.009650896	0.773319	0.479153
98	0.283394	5.703546137	0.344898	0.155815
99	0.347649	3.680401637	–0.908474	–1.448376
100	0.216045	1.480675236	0.953663	0.855934

According to Figure 13 and Figure 14, one can conclude that the predicted curve of the MLP deviates significantly from actual values, the prediction deviation range is –10–10 mm/min, the fluctuation range is large, and the prediction effect is poor. The prediction curve of the GRU model and LSTM model are nearer to the real value than that of MLP model, but the deviation still fluctuates in the range of –5–2 mm/min, and there is still a problem of poor prediction effect. The SSA-GRU model's predicted values are nearest to actual values, and the prediction error is stable between 0–0.6mm/min. The detailed prediction error data of the above models are shown in Table 3. The model has excellent predictive precision and superior predictive performance.

From the above-mentioned discussion, the following conclusions can be drawn SSA-GRU model offers superior predictive precision over the GRU model, the MLP model, and the LSTM model, which can complete the shield machine propulsion speed prediction task well.

6.3 *Controlling effect of propulsion speed prediction value on sealed cabin pressure*

Under the actual working conditions, precisely regulating the shield machine propulsion speed is meaningful for the stability of the excavation surface. Therefore, a sealed cabin pressure control model is built by a neural network, the propulsion speed prediction value is used for it, and the effectiveness of the propulsion speed prediction value of SSA-GRU model is further tested by examining the controlling effectiveness of the sealed cabin pressure at all monitored stations. Figure 15 presents the spread of each monitored spot in a sealed cabin. The controlling effectiveness for the propulsion speed predicted value of SSA-GRU on the sealed cabin pressure at all monitored spots is illustrated in Figures 16–19, and the sealed cabin pressure error value at each monitoring point is depicted in Figure 19.

Figure 15 Sealed cabin pressure monitoring point distribution (see online version for colours)

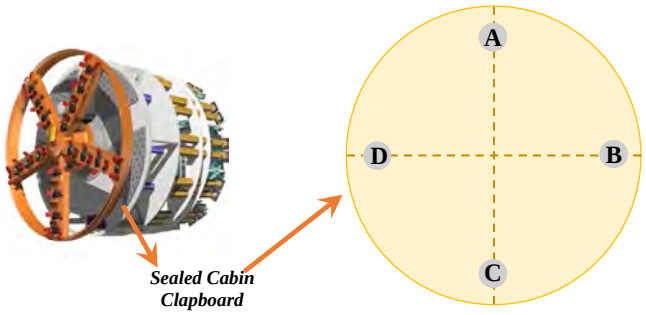

Figure 16 Pressure control effect for sealed cabin monitoring spot A (see online version for colours)

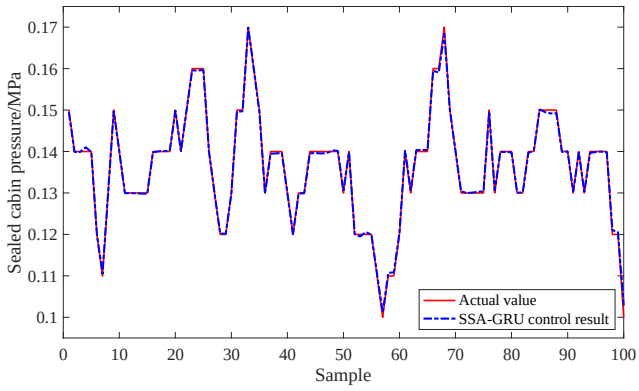

According to Figures 16–19, it can be concluded that the blue dashed line represents the control curve of prediction propulsion speed on sealed cabin pressure at each point obtained by SSA-GRU model. The red line represents sealed cabin pressure values in practical operating situations. The two curves at four monitoring spots, A, B, C, and D, are well-fitted, and sealed cabin pressure error values at each monitoring point are all within the error allowable range in practical operating situations, which could illustrate that propulsion speed prediction from the SSA-GRU model

allows precisely controlled sealed cabin pressure with very little error.

Figure 17 Pressure control effect for sealed cabin monitoring spot B (see online version for colours)

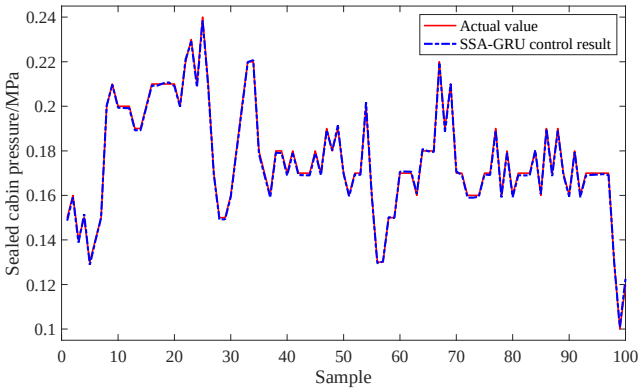

Figure 18 Pressure control effect for sealed cabin monitoring spot C (see online version for colours)

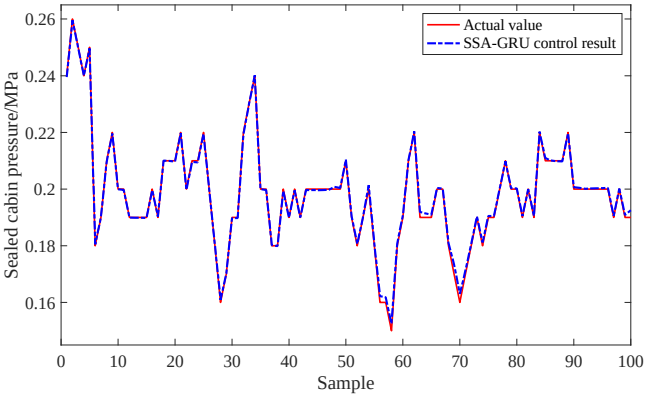

Figure 19 Pressure control effect for sealed cabin monitoring spot D (see online version for colours)

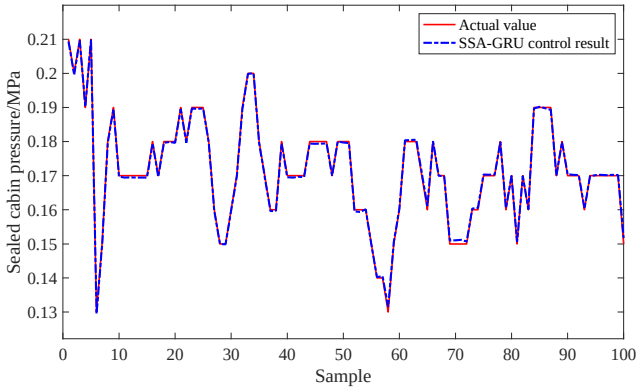

Based on the above analysis, it can be obtained that the propulsive speed prediction value of SSA-GRU has better controlling effectiveness on sealed cabin pressure at each monitoring point, which can indicate the effectiveness of the propulsive speed prediction value of SSA-GRU.

Figure 20 Prediction pressure error values for each monitoring point (see online version for colours)

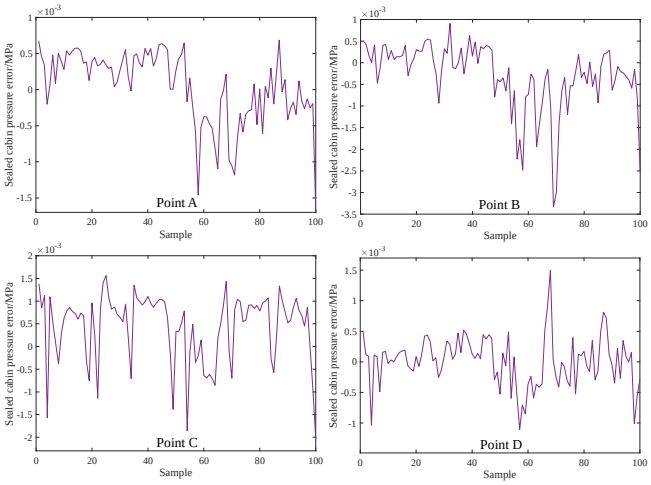

7 Conclusions

This paper proposes a shield machine propulsion speed prediction scheme based on SSA-GRU. SSA obtains the best hyperparameters of the GRU model through global search for optimisation and verifies that the hyperparameters searched in SSA allow for fast convergence in the predictive model via observation of the variation in the loss function of SSA-GRU during the training process. The simulation findings demonstrate:

1 SSA-GRU propulsion speed prediction model has high prediction precision, and the error between prediction value and actual value is small, which can fulfil the prediction task well.

2 Compared with other prediction models, the SSA-GRU model has a better predictive effect, smaller error value, and higher prediction performance.

3 The prediction propulsion speed obtained by the SSA-GRU model can accurately regulate sealed cabin pressure at each monitoring point. This study offers references for shield machine drivers in accurately regulating the propulsion speed and realises the coordinated control for multiple systems of the shield machine, which improves the working efficiency and intelligence level.

Acknowledgements

The paper is supported by the Basic Scientific Research Program of The Educational Department of Liaoning Province of China–General Program (Grant No. LJKMZ20220730), Scientific Research Fund Program of The Educational Department of Liaoning Province of China (Grant No. L2019018).

This research has successfully applied deep learning technology in the field of predictive control of earth-pressure-balanced shields, realising real-time prediction of shield tunnelling speed. It provides a new path for the development of AI technology in tunnel construction.

References

Armaghani, D.J., Koopialipoor, M., Marto, A. and Yagiz, S. (2019) 'Application of several optimization techniques for estimating TBM advance rate in granitic rocks', *Journal of Rock Mechanics and Geotechnical Engineering*, Vol. 11, No. 4, pp.779–789.

Chen, H., Xiao, C., Yao, Z., Jiang, H., Zhang, T. and Guan, Y. (2019a) 'Prediction of TBM tunnelling parameters through an LSTM neural network', *2019 IEEE International Conference on Robotics and Biomimetics (ROBIO)*.

Chen, R-P., Lin, X-T. and Wu, H-N. (2019b) 'An analytical model to predict the limit support pressure on a deep shield tunnel face', *Computers and Geotechnics*, Vol. 115, No. 11, p.103174.

Chen, L., Hashiba, K., Liu, Z., Lin, F. and Mao, W. (2023) 'Spatial-temporal fusion network for maximum ground surface settlement prediction during tunnel excavation', *Autom. Constr. Automation in Construction*, Vol. 147, p.104732, https://doi.org/10.1016/J.AUTCON.2022.104732.

Guo, S., Wang, B., Zhang, P., Wang, S., Guo, Z. and Hou, X. (2023) 'Influence analysis and relationship evolution between construction parameters and ground settlements induced by shield tunnelling under soil-rock mixed-face conditions', *Tunn. Undergr. Space Technol.*, Vol. 134, p.105020, https://doi.org/10.1016/J.TUST.2023.105020.

Huang, H.W., Chang, J.Q., Zhang, D.M., Zhang, J., Wu, H. M. and Li, G. (2022) 'Machine learning-based automatic control of tunnelling posture of shield machine', *J. Rock Mech. Geotech. Eng.*, Vol. 14, No. 4, pp.1153–1164, https://doi.org/10.1016/J.JRMGE.2022.06.001.

Hussaine, S.M. and Mu, L.L. (2022) 'Intelligent prediction of maximum ground settlement induced by EPB shield tunnelling using automated machine learning techniques', *Mathematics*, Vol. 10, No. 24, p.4637, https://doi.org/10.3390/MATH10244637.

Kongshu, D., Xiaoqiang, T., Liping, W. and Xu, C. (2011) 'Force transmission characteristics for the non-equidistant arrangement thrust systems of shield tunnelling machines', *Automation in Construction*, Vol. 20, No. 5, pp.588–595.

Li, X. and Gong, G. (2019) 'Predictive control of slurry pressure balance in shield tunnelling using diagonal recurrent neural network and evolved particle swarm optimization', *Automation in Construction*, Vol. 107, No. 11, p.102928.

Li, X. and Gong, G. (2020) 'Objective-oriented genetic algorithm based dynamical sliding mode control for slurry level and air pressure in shield tunnelling', *Automation in Construction*, Vol. 109, No. 1, p.102987.

Liu, X., Wang, Z.W., Wang, Y.D., Shao, C. and Cong, Q.M. (2022b) 'Predicting variation of multipoint earth pressure in sealed chambers of shield tunnelling machines based on hybrid deep learning', *Autom. Constr.*, Vol. 143, p.104567, https://doi.org/10.1016/J.AUTCON.2022.104567.

Liu, X-Y., Gan, X-Y., Shao, C., Wang, Y-D. and Cong, Q-M. (2022a) 'CNN-GRU-based intelligent online prediction of screw machine rotation speed for earth pressure balance shield machine', *Engineering Research Express*, Vol. 4, No. 4, p.45021, https://doi.org/10.1088/2631-8695/ACA1F9.

Liu, Y., Wang, L., Li, D. and Wang, K. (2023) 'State-of-health estimation of lithium-ion batteries based on electrochemical impedance spectroscopy: a review', *Protection and Control of Modern Power Systems*, Vol. 8, No. 3, pp.1–17.

Ma, N., Yin, H. and Wang, K. (2023) 'Prediction of the remaining useful life of supercapacitors at different temperatures based on improved long short-term memory', *Energies*, Vol. 16, No. 14, p.5240.

Pan, Y. and Zhang, L.M. (2022) 'Mitigating tunnel-induced damages using deep neural networks', *Autom. Constr.*, Vol. 138, p.104219, https://doi.org/10.1016/J.AUTCON.2022.104219.

Qin, H.Y., Tan, P.L., Chen, Z.Q., Sun, M.W. and Sun, Q.L. (2022) 'Deep reinforcement learning based active disturbance rejection control for ship course control', *Neurocomputing*, Vol. 484, pp.99–108, https://doi.org/10.1016/J.NEUCOM.2021.06.096.

Song, X., Shi, M., Wu, J. and Sun, W. (2019) 'A new fuzzy c-means clustering-based time series segmentation approach and its application on tunnel boring machine analysis', *Mechanical Systems and Signal Processing*, Vol. 133, No. 20, p.106279.

Yeh, I-C. (1997) 'Application of neural networks to automatic soil pressure balance control for shield tunnelling', *Automation in Construction*, Vol. 5, No. 5, pp.421–426.

Yi, Z., Chen, Z., Yin, K., Wang, L. and Wang, K. (2023) 'Sensing as the key to the safety and sustainability of new energy storage devices', *Protection and Control of Modern Power Systems*, Vol. 8, No. 1, pp.1–22.

Yu, H., Tao, J., Huang, S., Qin, C., Xiao, D. and Liu, C. (2021) 'A field parameters-based method for real-time wear estimation of disc cutter on TBM cutterhead', *Automation in Construction*, Vol. 124, No. 4, p.103603.

Yu, X., Shang, Y., Zheng, L. and Wang, K. (2023) 'Application of nanogenerators in the field of acoustics', *ACS Applied Electronic Materials*, Vol. 5, No. 9, pp.5240–5248.

Zhang, W., Liu, X., Zhang, L. and Wang, Y. (2023) 'Intelligent real-time prediction of multi-region thrust of EPB shield machine based on SSA-LSTM', *Engineering Research Express*, Vol. 5, No. 3, https://doi.org/10.1088/2631-8695/ace3a5.